metals

MDPI

Article

Effects of Temperature on Axial Crushing Behavior of Circular Multi-Walled Tubes

Zhijia Zhang [1,*], Ruixuan Feng [1], Yongjing Wang [2], Lijun Zhang [1] and Qiancheng Zhang [1,*]

[1] State Key Laboratory for Strength and Vibration of Mechanical Structures, Xi'an Jiaotong University, Xi'an 710049, China
[2] State Key Laboratory for Mechanical Behavior of Materials, Xi'an Jiaotong University, Xi'an 710049, China
* Correspondence: zhijiazhang187@xjtu.edu.cn (Z.Z.); zqc111999@xjtu.edu.cn (Q.Z.)

Abstract: In this work, the impact of temperature on the crushing performance of multi-walled tube (MWT) were investigated using a combined experimental, theoretical and numerical method. The MWT was fabricated using extrusion technology, and the temperature-dependent axial crushing experiment was performed on a hydraulic testing machine. The results show that the peak crushing force (PCF), the mean force (P_m) and the specific energy absorption (SEA) decreased near-linearly by 21.7%, 30.7% and 30.7% as the temperature increased from 25 °C to 250 °C, while the crushing load efficiency (CLE) was insensitive to temperature. The average forces obtained via numerical prediction, theoretical analysis and experimental testing were basically consistent. The numerical results indicate that varied temperature alters the number of dominant wavelets and the relative lateral deflections of MWT. In addition, compared with the competitive structures, the energy absorption property of MWT is excellent at high temperatures.

Keywords: multi-walled tube; crushing performance; elevated temperature; energy absorption

Citation: Zhang, Z.; Feng, R.; Wang, Y.; Zhang, L.; Zhang, Q. Effects of Temperature on Axial Crushing Behavior of Circular Multi-Walled Tubes. *Metals* **2023**, *13*, 1976. https://doi.org/10.3390/met13121976

Academic Editors: Umberto Prisco and Sergei Alexandrov

Received: 4 October 2023
Revised: 14 November 2023
Accepted: 16 November 2023
Published: 5 December 2023

1. Introduction

A major challenge in civil engineering, automotive engineering and aerospace engineering is to design various types of lightweight, low-cost and anti-collision structures with high energy absorption capabilities to ensure the safety of instruments and passengers [1–3]. In recent years, metal thin-walled tubes, as energy absorbing devices, have been extensively studied due to their advantages of being simple to manufacture and having outstanding energy absorption performance and stable deformation modes under crushing force [4,5]. For the sake of elevating the energy-absorbing performance of thin-walled tubes, varied cross-section configurations such as square [6,7], circle [8], triangle [9] and other cross-sectional shapes [10,11] were designed. These studies showed that, compared with the other cross-section structures, circular cross-section tubes have better energy absorption performance and offer better load uniformity against axial and oblique load [12].

The main factors affecting the energy absorption properties of such tube components are material properties and structural geometry. Due to good ductility, metal materials, such as aluminum alloy and stainless steel, are the most commonly employed materials for the fabrication of these tubes. Bhutada [13] found that the strengths of AA6061 T6 and AA7108 T6 are stronger than that of the steel DP600 alloy at same weight. The performance of the A17108T6 alloy is superior to that of the A16061T6 alloy. It can achieve more energy absorption within a limited crushing distance. A17108T6 has increased the buckling load of the collision tank and bumper crossbeam. This alloy has the impact of reducing the bending of the bumper crossbeam and introducing greater loads to the collision tank. Even if a higher strength A17108T6 alloy is used, the deformation of the collision tank is increased and occurs earlier than that of the lower strength A16061T6 collision tank. Simhachalam et al. [14] revealed that the AA7005 tube had minimal changes in specific energy absorption, CFE, peak force, and average force. The CFE change varied between 0.54 and 0.48, with

a 6% rate of change between samples. The SEA alters between 51 and 53 kJ/kg, with a variation of 4% between samples. The average force in the experiment was 27 kN, which changed by 2.9% compared to the theoretical prediction. The deformation mode of AA7005 shows progressive folding and axisymmetric rings in both compression tests and static simulations. The experimental crushing test and the numerical simulation prediction of AA7005 tube was also very consistent in force-displacement results, except that the peak force was higher than the numerical prediction. The average force obtained via numerical prediction was 25.7 kN, which changed by 4.6% compared to the experimental results. For thin-walled tubes, the energy dissipation mechanism was identified through the local folding and bending deformation of metal materials, that is, the energy dissipation is usually concentrated in a relatively narrow area of structure; however, the rest only has rigid motion, resulting in the low utilization rate of plastic deformation and limited energy absorption efficiency [4].

For the sake of further elevating the energy absorption performance of thin-walled structure, the design concept of a multi-wall element is used to enhance the crashworthy capability of thin-walled structures, which has a simpler fabrication process and provides better weight efficiency than adding foam and inner tube [15–17]. Kim et al. [18] revealed that multi-walled tubes exhibited a marked improvement in collision energy absorption and weight efficiency compared to traditional single tubes.

The results indicate that the SEA of the proposed tube is 1.9 times higher than that of the corresponding single tube. Zhang [19] studied experimentally and numerically the compression behavior of multi-walled tubes with varied cross-sections. It was found that multi-walled tubes were more efficient than a single tube in specific energy absorption. The SEA of multi-walled tubes can be enhanced by 120–220%, relative to single tubes. In addition, other multi-walled tubes inspired by the micro-structure of biological tissues have also been demonstrated to elevate the crashworthiness performance [20–24]. All these studies show that the crashworthy performance of multi-walled tubes can outperform a single tube. Many works have been carried out to clarify why the energy absorption performance of multi-walled tubes is higher than that of single tubes by using experimental tests [25], theoretical analyses [26] and numerical simulations [27]. Adding a multi-cell wall alters the deformation mode of thin-walled tubes and causes more elements to participate in plastic deformation and energy dissipation [28].

Multi-walled tubes can operate at high temperatures and are required for a range of critical structural engineering applications, such as construction, automotive and aerospace. At present, the research on the crashworthiness behavior of thin-walled metal tubes mainly focuses on room temperature; however, the crushing deformation of thin-walled metallic tubes is sensitive to temperature [29]. Dipaolo [30] investigated the impact of ambient temperature on the crushing behavior of square tubes. The results revealed that the loading and energy absorption capability of the secondary folded phase are significantly affected by ambient temperature. Tian [31] theoretically predicted the impact of a high-temperature environment on the crushing performance of a metal sandwich tube. It is shown that the average crushing loading of sandwich tubes gradually reduces as the temperature increases.

Overall, previous research has found that multi-walled tubes have better energy absorption performance and mass efficiency than a single tube at room temperature; however, according to the authors' knowledge, until now there have been no studies focusing on the crushing performance of MWTs under high temperatures. In this paper, the effect of temperature on crushing behavior and the energy absorption performance of MWTs are investigated using a combination of experimental testing, numerical prediction and theoretical methods. Moreover, the effect of geometrical parameters on energy absorption performance are clarified.

2. Temperature-Dependent Model of a Multi-Walled Tube

As shown in Figure 1, a MWT was prepared in this study to investigate the axial crushing behavior at different temperatures. The geometric characteristics of the MWT

are as follows: inside diameter d, height H, tube wall thickness t_r and the thickness of multi-walled wall is t_c. In this work, the units for all quantities included in the equations are in millimeters (mm).

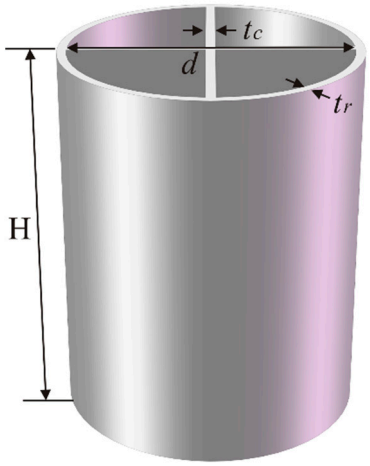

Figure 1. Geometric parameters of the MWT.

2.1. Energy Absorbed by Multi-Walled Tubes

In this work, the simplified super folding element method was used to evaluate the mean crushing loading of a multi-walled tube. A complete fold was used for analysis and the length of each folded wave is assumed to be $2H_F$. The external wall was dissipated by bending energy and membrane energy in thin-walled tubes.

The energy balance condition is written as

$$2P_m(T)H_F\kappa = W_{\text{bending}} + W_{\text{membrance}} \tag{1}$$

where $P_m(T)$, W_{bending} and $W_{\text{membrance}}$ are the mean crushing loading, bending energy and membrane energy, respectively. In a complete fold, an effective crushing distance coefficient k is added into Equation (1), which changes between 0.65 and 0.75 for multi-walled tubes [32]. In this work, the value of k is regarded as the average value between 0.65 and 0.75, and 0.7 is employed for all walls.

2.2. Bending Energy

The shape of the deformation zone is shown in Figure 2. Each element contains three line segments: two arcs of equal radius, connected by lines tangential to the arcs. By definition, the length of all four arcs is equal to the effective hinge length, aH. Note that H is the semi-plastic wavelength that will be determined in the analysis. For simplicity, no variation of H is assumed during the collapse. At a given axial crushing distance, the shape and instantaneous position of the deformation zone is defined by either the instantaneous radii, r_1 and r_2, or the two angles, α and β. The bending energy W_{bending} is obtained by summing up the dissipated energy at stationary hinge lines. Therefore, the bending energy is written as [33]:

$$W_{\text{bending}} = 2\pi M_0 L_c \tag{2}$$

where L_c is the length of sectional profile and M_0 is the full plastic bending moment per unit length and can be obtained as follows:

$$M_0 = \sigma_0(T) \quad t^2/4 \tag{3}$$

where t is wall thickness ($t = t_r$ or t_c.) and $\sigma_0(T)$ is the flow stress of base material at temperature T, which can be expressed as

$$\sigma_0(T) = 0.5\big(\sigma_y(T) + \sigma_u(T)\big) \tag{4}$$

where $\sigma_y(T)$ and $\sigma_u(T)$ are, respectively, the yield strength and the ultimate strength of the base materials.

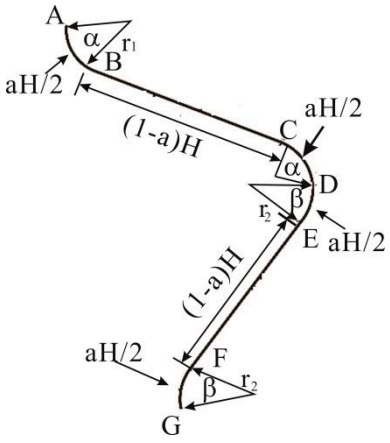

Figure 2. Cross-section of embedded tube.

2.3. Membrane Energy

In the present study, the MWT is composed of three component elements, namely the shell angle element, the concave T-shaped element and the cross element, as shown in Figure 3. The total membrane energy is obtained by adding the membrane energy of all the constituent elements. According to Zhang's model [34], in stretch mode, the membrane energy consumption at the corner is

$$W_{membrane} = W^{CE}_{membrane} + W^{TPE}_{membrane} + W^{CFE}_{membrane} \tag{5}$$

$$W^{CE}_{membrane} = 2M_0\Delta S/r'(\theta) \tag{6}$$

where ΔS, $r'(\theta)$ and M_0 are the area of static hinge deformation, the fully plastic bending moment and the hinge bending radius of curvature, respectively, and can be obtained as follows:

$$\Delta S = H^2 \tan\theta/2 \tag{7}$$

$$r'(\theta) = a_1 B^{a_2} t^{1-a_2}(\tan(\theta/2) + a_3/\tan(\theta/2)) \tag{8}$$

where H is the folded wavelength of the unit and θ is between folded units.a_1, a_2, a_3 are constants, and B is the length of the other side of the folding unit.

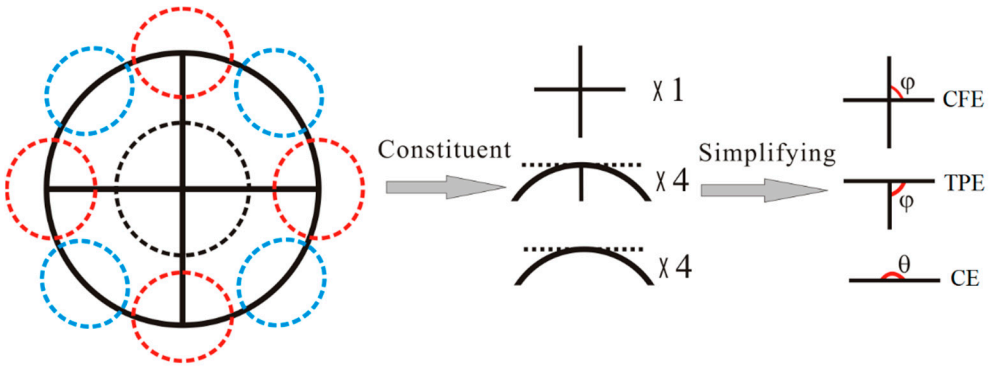

Figure 3. Division and simplification of multi-walled tube.

The T-shape element is a three-plate element. A three-plate element consists of a corner element with a central angle 2ϕ and an addition plate for inserting the symmetry

plane of the corner element. According to Zhang [33], the membrane energy dissipated by the additional plate is as follows:

$$W_{membrane}^{TPE} = 2M_0H^2\left[\frac{4\tan(\varphi/2)}{t} + \frac{\tan\varphi}{a_1B^{a_2}t^{1-a_2}(\tan\varphi + a_3/\tan\varphi)}\right] \quad (9)$$

where φ is the angle between two adjacent plates.

The membrane energy dissipated and the crisscross element is calculated as follows [34]:

$$W_{membrane}^{CFE} = \frac{8}{3}M_0H^2\left(\frac{\tan\varphi}{a_1B^{a_2}t^{1-a_2}(\tan\varphi + a_3/\tan\varphi)} + \frac{4\tan(\varphi/2)}{t}\right) \quad (10)$$

The half-folded wavelength can be acquired via

$$\frac{\partial P_m(T)}{\partial H_F} = 0 \quad (11)$$

The energy balance equation can be written as

$$\begin{aligned} &2\pi M_0L_c + 2N_1M_0\Delta S/\mathrm{r}'(\theta) + 2N_2M_0H^2\left[\frac{4\tan(\varphi/2)}{t} + \frac{\tan\varphi}{a_1B^{a_2}t^{1-a_2}(\tan\varphi+a_3/\tan\varphi)}\right] \\ &+\frac{8}{3}N_3M_0H^2\left(\frac{\tan\varphi}{a_1B^{a_2}t^{1-a_2}(\tan\varphi+a_3/\tan\varphi)} + \frac{4\tan(\varphi/2)}{t}\right) - 2H_F\kappa P_m(T) = 0 \end{aligned} \quad (12)$$

3. Experiment

3.1. Materials and Fabrication

In this study, the direct hot extrusion method was used. A schematic representation of the process is shown in Figure 1. In the process, the billet is heated to the required temperature first, and then it is extruded along the same direction of the ram or punch. Frictions between die and billet and mandrel and billet are quite important. In the hot extrusion process, several factors affect temperature variation: flow stress versus strain based on temperature and strain rate, plastic deformation (homogenous and redundant work) and friction coefficient. The 6061 aluminum alloy (Al—1.12; Mg—0.65; Si—0.23; Fe—0.015; Mn—0.19; Cu—0.09; Cr—0.023; Ti—0.18; Zn—0.014; Ca) in the tube extrusion was employed in a MWT in this work. The MWT was prepared under the extrusion conditions of billet homogenization at 450 °C for 8 h, pre-heating at 450 °C, with an extrusion speed of 25 cm/s, in the 150-ton hydraulic press machine (Shandong Xingchen Pipe Industry Co., Ltd., Rizhao City, China). Extruded MWT specimens are shown in Figure 4. The mass and dimensions of the prepared specimens are listed in Table 1.

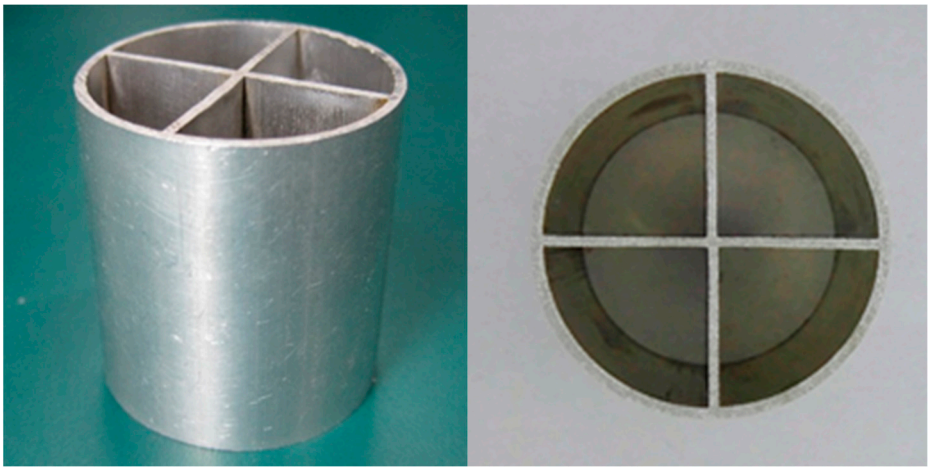

Figure 4. MWT specimens for experimental tests.

Table 1. Mass and dimensions of the fabricated specimens (mm).

Specimen	Mass (g)	d	t_c	t_r	H
MWT	18.01	15	1	1	42

3.2. Test Setup and Equipment

The axial quasi-static crushing test was performed on a hydraulic testing machine (MTS-880, MTS Corporation, 100 kN) with an environmental chamber (the temperature had an upper limit of 400 °C), as shown in Figure 5. The tested specimens were heated at a speed of 5 °C/min until the test temperatures (25 °C, 150 °C and 250 °C) were reached. All samples were placed in an ambient chamber and kept for 30 min to keep the temperature uniform inside the samples. The MWT was loaded at 1 mm/min until it was compacted. The loading-displacement curve was obtained by a computer system, and the deformation process was captured by high-definition cameras. To ensure repeatability at each target temperature, the three repetitive tests of samples were conducted.

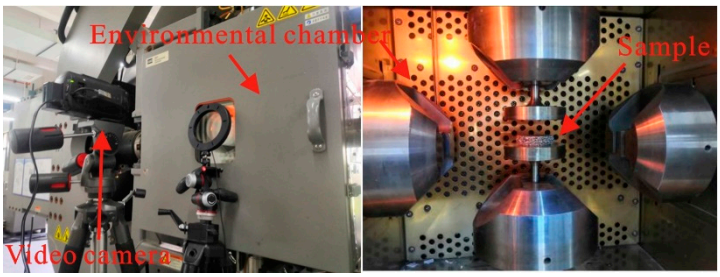

Figure 5. Test setup and equipment.

4. Numerical Modeling

The commercial code ABAQUS/Explicit was used to investigate the influence of temperature on the crushing behavior of specimens. In numerical models, as displayed in Figure 6, four-node shell elements (S4R) were employed to discretize the multi-walled tube and the upper and lower rigid plates. The lower rigid plate is fixed, while the upper rigid wall is constrained in all degrees of freedom except three directions. The moving rigid wall moved downward at a speed of 2 mm/min to guarantee that the crushing behavior was quasi-static. The node surface contact algorithm was used to model the contact between the tube and the rigid plate, while the automatic single surface contact algorithm was used to model the contact of the tube itself. The friction coefficient was set as 0.2. To ensure calculation accuracy while reducing calculation costs, the average size of the MWT was 0.5 mm. The Al 6061's material properties employed in the simulation model are listed in Table 2.

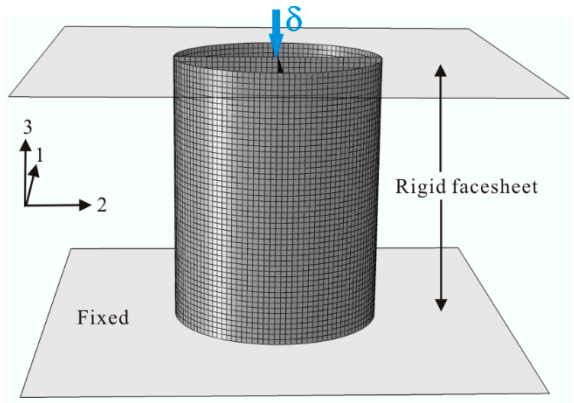

Figure 6. Simulation model of the multi-walled tube.

Table 2. The Al 6061 material parameters used in the simulation model.

Temperature (°C)	Young's Modulus (MPa)	Yield Strength (MPa)	Poisson's Ratio
25	70,000	175	0.3
150	65,300	165	0.3
250	53,000	136	0.3

5. Results and Discussion

5.1. Crush Response

Figure 7a–c show the crushing loading–displacement curves of MWTs under varied temperatures. All the loading–displacement curves present the similar trends with five typical features: an initial linear elastic region, a non-linear increasing until the yield point, a maximal force drop after yielding, a force fluctuation region with wave crests and a densification region with rapidly increasing force. Generally, every force drop corresponds with a fold formation.

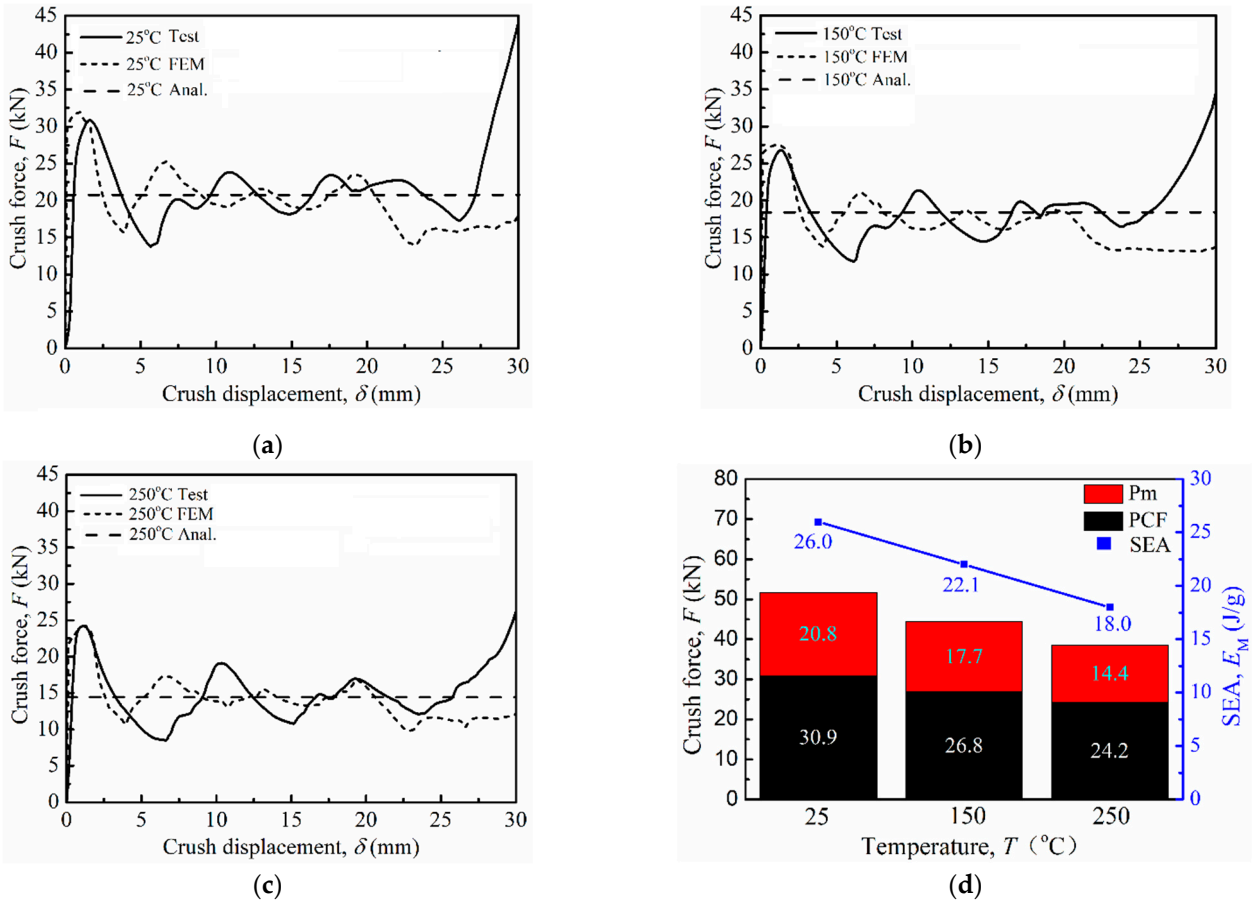

Figure 7. Crushing loading–displacement curves of tested specimens: (**a**) 25 °C; (**b**) 150 °C; (**c**) 250 °C; (**d**) the average force and specific energy absorption at varied temperatures.

The peak crushing force (PCF), average force (P_m) and specific energy absorption (SEA) decrease near-linearly, as shown in Figure 7d, by 21.7%, 30.7% and 30.7% as the temperature rises from 25 °C to 250 °C. This decrease in material properties is mainly caused by a thermal softening effect. The temperatures have an obvious influence on the crushing performance and energy absorption capabilities of MWT.

Figure 8 shows sequential pictures of MWTs during the crushing process under different temperatures. It can be seen that the deformation history of all specimens under varied

temperatures are similar: failure occurs preferentially near the upper plate, accompanied by a concertina-like mode, and the distal end is barely deformed. Then, a regular and successive fold occurs at the bottom of the first folds as the crushing displacement increases.

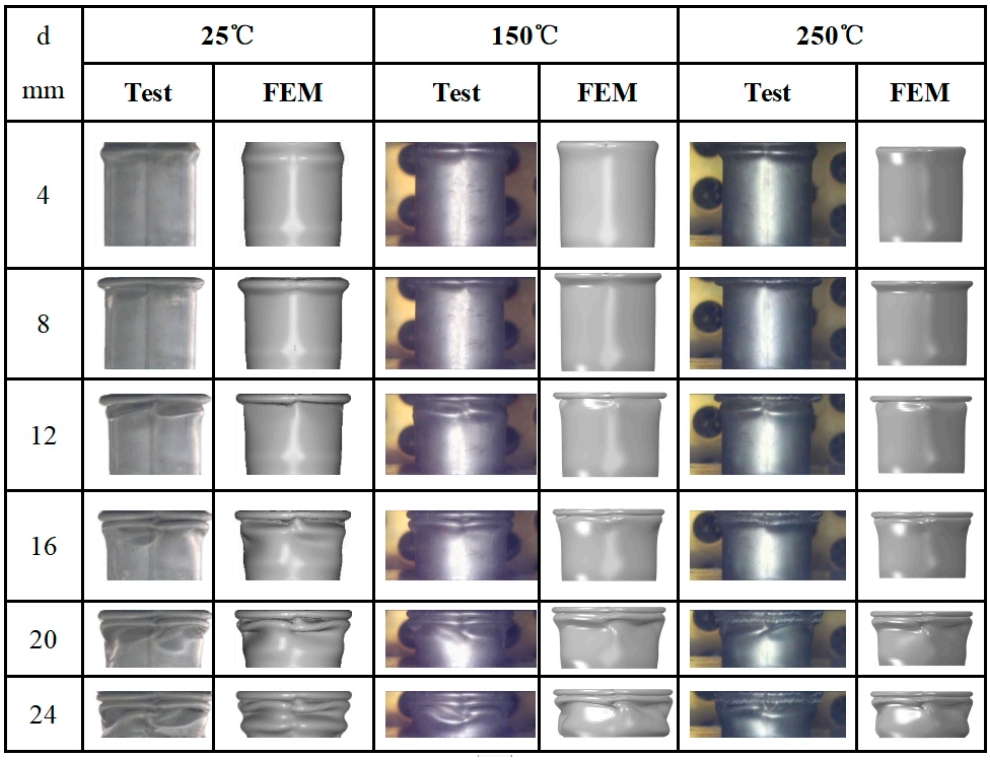

Figure 8. Deformation history of specimens at various temperatures.

5.2. Validation

Figures 7–9 and Table 3 show the comparison between FE predictions, experimental results and theoretical analysis for crushing performance and energy absorption. It was found that, during the crushing process, the crushing force fluctuation obtained by the FE predictions is close to the experimental results, and the finite element models well describe the deformation mode of MWTs at different temperatures in Figures 8 and 9. It can also be seen that a good agreement between the average forces is obtained, as observed through finite element prediction, theoretical analysis and experimental testing (Figure 7 and Table 3). Therefore, the numerical simulation model employed in this study is convenient and accurate and can be employed to research the crushing performance of MWTss at varied temperatures.

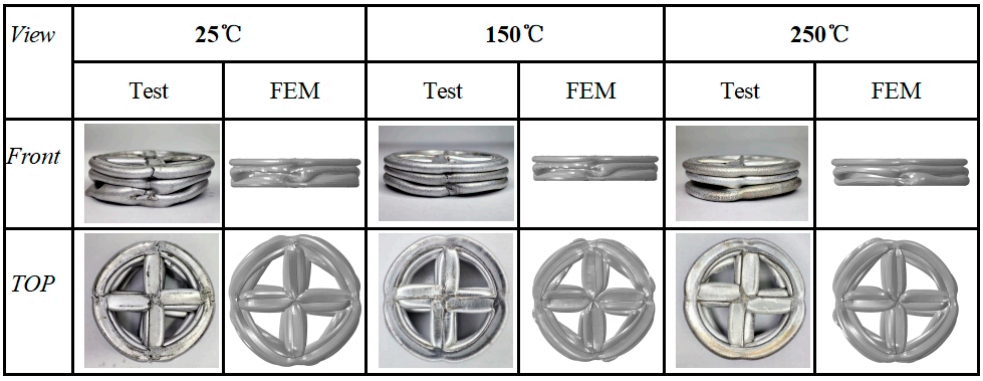

Figure 9. Experimental results and numerical simulation of crushing collapse at various temperatures.

Table 3. The energy absorption parameters for samples at varied temperatures.

Temperature (°C)	Type of Result	PCF (kN)	Pm (kN)	SEA (J/g)	CFE (%)
25	Test	30.88	20.79	25.99	67.32
	FEM	31.9	21.5	26.87	67.39
	Theoretical	-	21.42	26.77	-
150	Test	26.80	17.70	22.14	66.04
	FEM	27.4	17.9	22.39	65.33
	Theoretical	-	17.83	22.30	-
250	Test	24.19	14.36	17.95	59.36
	FEM	24.3	15.01	18.75	61.17
	Theoretical	-	14.6	18.25	-

5.3. Collapse Mechanisms

FE method is used to reveal the deformation morphologies of MWT in the crushing process and research the effect mechanism of temperature on the deformation morphology of MWT. The local coordinates of multi-walled tubes are shown in Figure 10. x/L indicates the relative position of a point on the selected path (o_1p_1 for the multi-cell wall and o_2p_2 for the tube wall) in MWT, whilst w is the lateral deflection of the selected point.

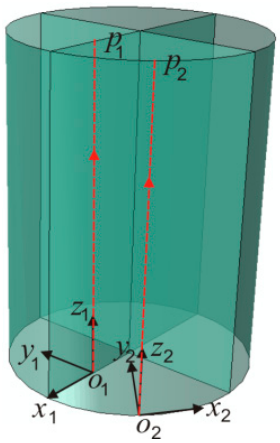

Figure 10. Definition of local coordinate system of MWT.

Figure 11 shows the lateral deflection—the relative position of the selected point in the multi-cell wall. It can be seen that when the crushing displacement is 2.2 mm, there are two dominant wavelets near the end of the multi-cell wall; however, there is one dominant wavelet near the end of tube wall. The relative lateral deflections are almost the same under different temperatures. As crush displacement increases to 6.2 mm, the dominant wavelet does not change, but the relative lateral deflections of the multi-cell wall and the tube wall under 150 °C and 250 °C are larger than those under 25 °C. The main reason is attributed to the softening of the material at high temperatures. As the crushing displacement further increases to 12.2 mm, there are five dominant wavelets in the multi-cell wall but only four dominant wavelets in the tube wall. The number of dominant wavelets and the relative lateral deflections of the multi-cell wall and the tube wall under 150 °C and 250 °C are larger than those under 25 °C.

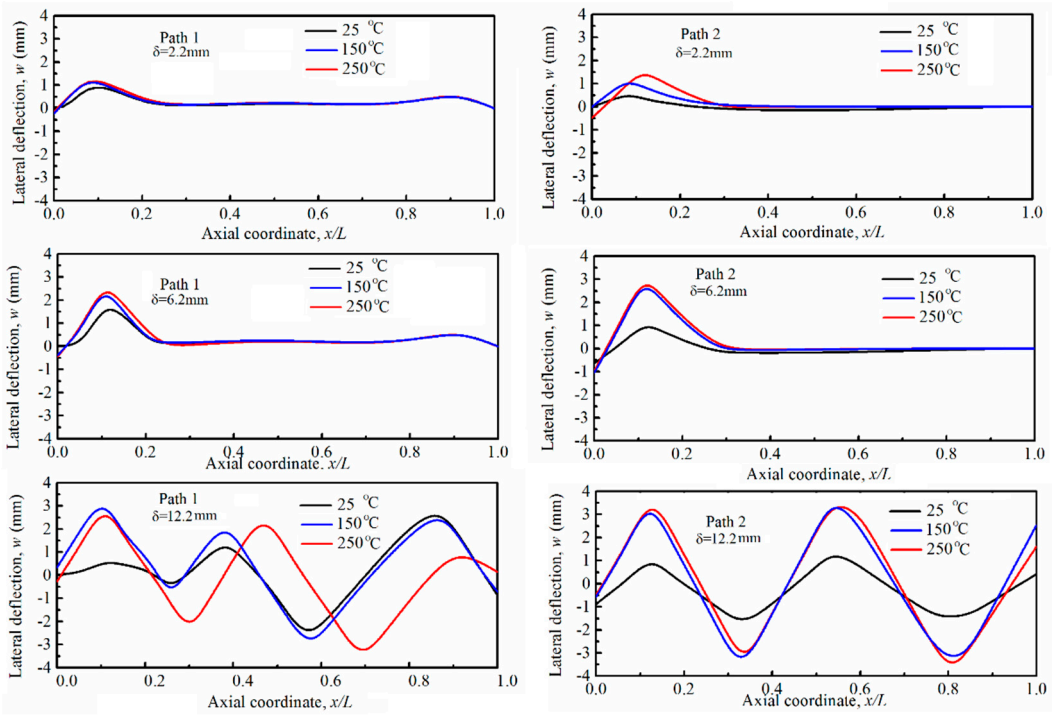

Figure 11. The lateral deflection of any a point on the selected path: (**a**) Path-1 and (**b**) Path-2 at different temperatures.

5.4. Parametric Simulations

In this section, the effects of key factors of multi-walled tubes on crushing behavior and energy absorption performance are researched using the FE method. The key geometrical parameters of MWTs are of a fixed value (H = 42 mm, d = 28 mm); however, the thickness of multi-walled tube changes. It can be seem that energy absorption parameters, including the peak crushing force (PCF), the mean crushing force (P_m), the crushing force efficiency (CFE), and the specific energy absorption (SEA), increase as the thickness of multi-walled tube increases but decrease as the temperature increases, as seen in Figure 12. The wall thickness of MWTs has an obvious impact on the energy absorption parameters of MWT.

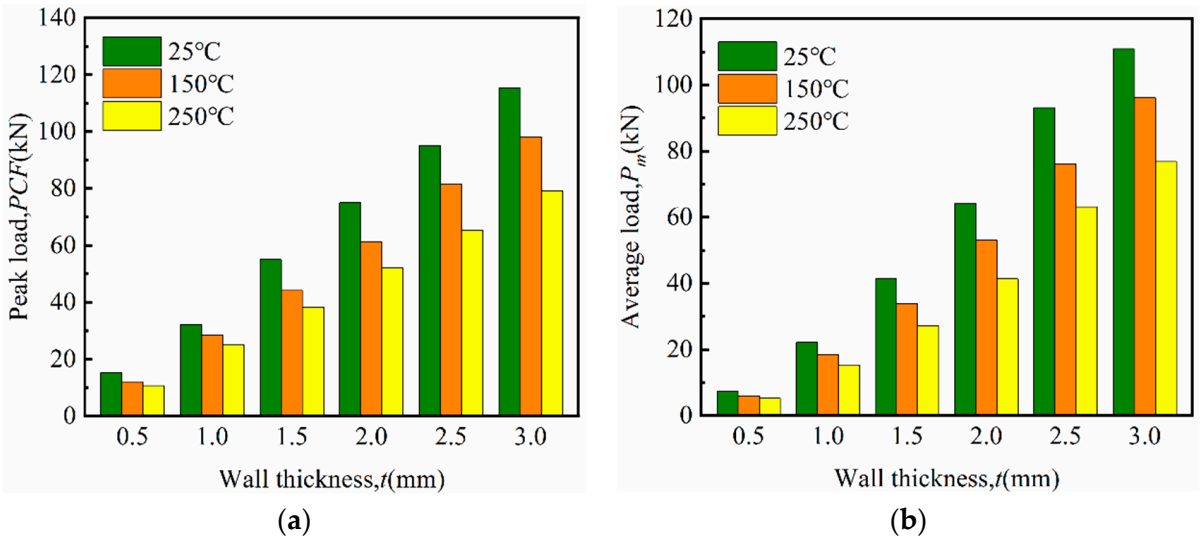

Figure 12. *Cont.*

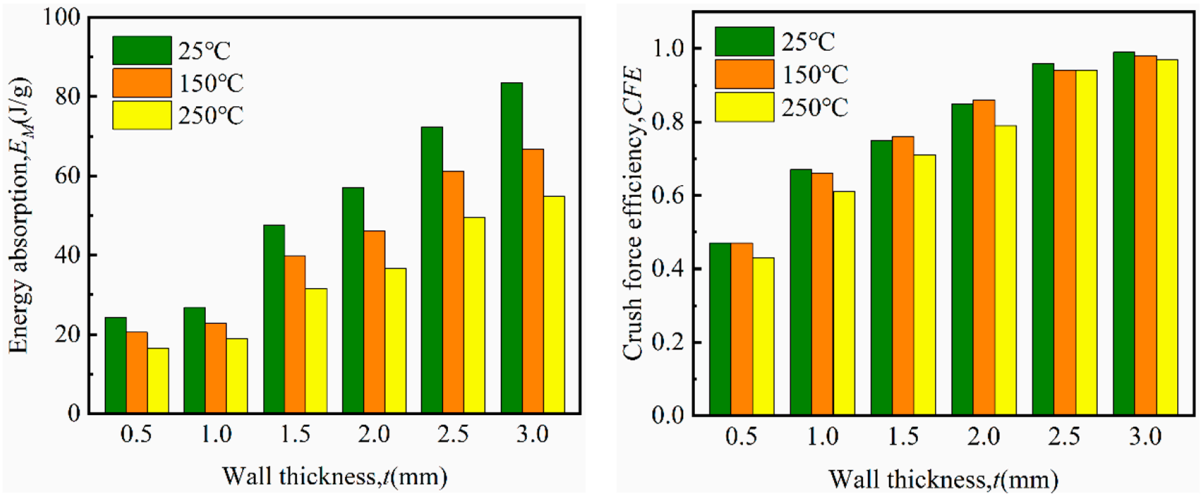

(**c**) (**d**)

Figure 12. Influence of wall thickness on (**a**) the peak load; (**b**) average load; (**c**) energy dissipation; (**d**) crush force efficiency.

6. Comparison with Competing Topologies

To compare the energy absorption performance of multi-walled tubes (MWTs) with competing structures at different temperatures, Figure 13 shows the experimentally measured specific energy absorption with unit mass and unit volume as functions of the temperature. Compared with foam [34–40], lattice [41], and foam-filled tube [42–44], it can be seen that the specific energy absorption of the MWT is prominent at high temperatures. In terms of loading capacity and energy absorption performance, the MWT is superior to metal foam.

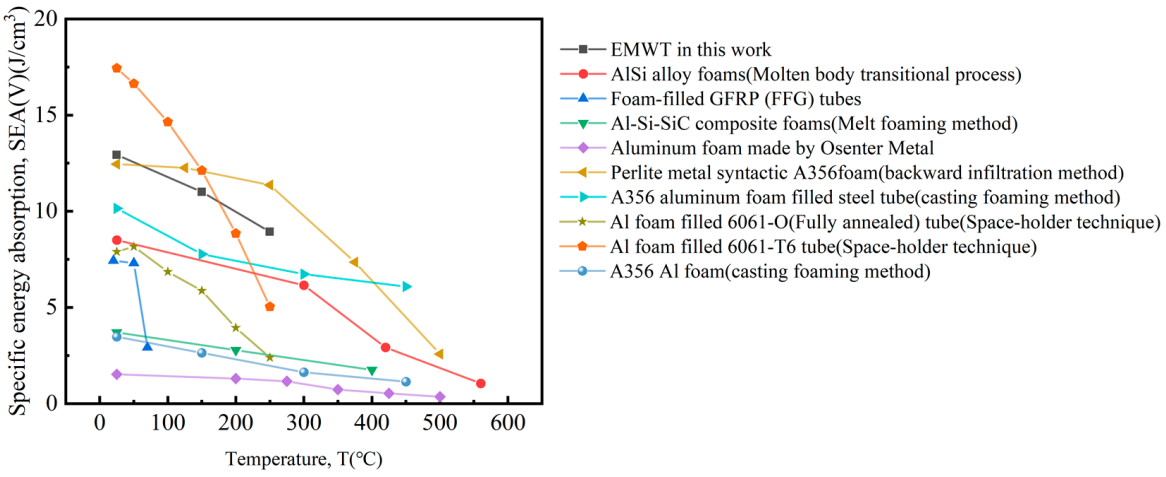

(**a**)

Figure 13. *Cont.*

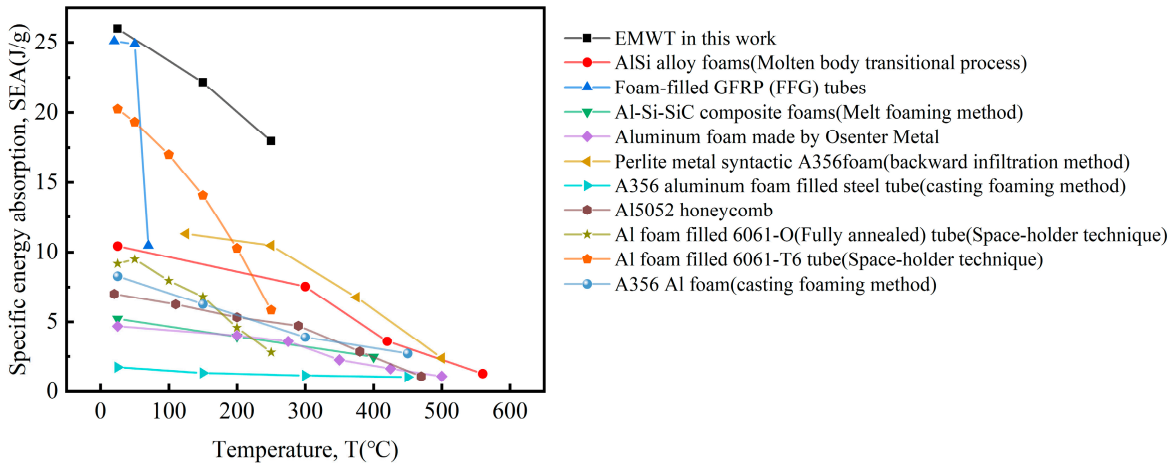

(**b**)

Figure 13. Comparison with competing structures: (**a**) energy absorption per unit volume; (**b**) energy absorption per unit mass.

7. Conclusions

In this research, the influence of high temperature on the crushing characteristics and energy absorption performance of multi-walled tubes (MWTs) are studied through experimental testing, theoretical analysis and FE predictions. It was shown that the peak crushing force (PCF), average force (P_m) and specific energy absorption (SEA) decrease near-linearly by 21.7%, 30.7% and 30.7% as the temperature increases from 25 °C to 250 °C. A good agreement between the average forces obtained via numerical simulation, theoretical analysis and experimental testing was achieved. The temperature had an impact on collapse mechanisms. The number of dominant wavelets and the relative lateral deflections of the cell wall and the tube wall under 150 °C and 250 °C were larger than that under 25 °C. The thicknesses of the multi-walled tubes have an effect on the crushing behaviors and the energy absorption capacity of MWTs. Compared with competing lattice materials and structures, the energy absorption performance of MWTs are more prominent at high temperatures on the material selection map.

Author Contributions: Methodology, Z.Z. and L.Z.; software, R.F. and L.Z.; validation, Z.Z.; formal analysis, R.F. and Y.W.; investigation, R.F. and Y.W.; writing—review and editing, R.F. and L.Z.; project administration, Q.Z.; funding acquisition, Q.Z. All authors have read and agreed to the published version of the manuscript.

Funding: This work was supported by the National Natural Science Foundation of China (12072250, 12102327, 12102328) and the China Postdoctoral Science Foundation, funded project (2020TQ0238, 2021M702606).

Data Availability Statement: All data are available from the corresponding author on reasonable request.

Conflicts of Interest: The authors declare no conflict of interest.

References

1. Ha, S.; Lu, G.X. Thin-walled corrugated structures: A review of crashworthiness designs and energy absorption characteristics. *Thin-Walled Struct.* **2020**, *157*, 106995. [CrossRef]
2. Zhang, Q.C.; Yang, X.H.; Li, P.; Huang, G.Y.; Feng, S.S.; Shen, C.; Han, B.; Zhang, X.H.; Jin, F.; Xu, F.; et al. Bioinspired engineering of honeycomb structure-using nature to inspire human innovation. *Prog. Mater. Sci.* **2015**, *74*, 332–400. [CrossRef]
3. Schneider, J.; Schiffer, A.; Hafeez, F.; Kumar, S. Dynamic crushing of tailored honeycombs realized via additive manufacturing. *Int. J. Mech. Sci.* **2022**, *219*, 107126.
4. Baroutaji, A.; Sajjia, M.; Olabi, A.G. On the crashworthiness performance of thin-walled energy absorbers: Recent advances and future developments. *Thin-Walled Struct.* **2017**, *118*, 137–163. [CrossRef]

5. Abdullah, N.A.Z.; Sani, M.S.M.; Salwani, M.S.; Husain, N.A. A review on crashworthinesss tudies of crash box structure. *Thin-Walled Struct.* **2020**, *153*, 106795. [CrossRef]
6. Ming, S.; Zhou, C.; Li, T.; Song, Z.; Wang, B. Energy absorption of thin-walled square tubes designed by kirigami approach. *Int. J. Mech. Sci.* **2019**, *157–158*, 150–164. [CrossRef]
7. Hussein, R.D.; Dong, R.; Lu, G.; Thomson, R. An energy dissipating mechanism for crushing square aluminium tubes. *Compos. Struct.* **2018**, *183*, 643–653. [CrossRef]
8. Xie, S.; Chen, P.; Wang, N.; Wang, J.; Du, X. Crashworthiness study of circular tubes subjected to radial extrusion under quasi-static loading. *Int. J. Mech. Sci.* **2021**, *192*, 106128. [CrossRef]
9. Ge, C.; Gao, Q.; Wang, L. Theoretical and numerical analysis of crashworthiness of elliptical thin-walled tube. *Int. J. Mech. Sci.* **2018**, *148*, 467–474. [CrossRef]
10. Yang, H.; Lei, H.; Lu, G.; Zhang, Z.; Li, X.; Liu, Y. Energy absorption and failure pattern of hybrid composite tubes under quasi-static axial compression. *Compos. Part B Eng.* **2020**, *198*, 108217. [CrossRef]
11. Deng, X.; Liu, W. Multi-objective optimization of thin-walled sandwich tubes with lateral corrugated tubes in the middle for energy absorption. *Thin-Walled Struct.* **2019**, *137*, 303–317. [CrossRef]
12. Nia, A.A.; Hamedani, J.H. Comparative analysis of energy absorption and deformations of thin walled tubes with various section geometries. *Thin-Walled Struct.* **2010**, *48*, 946–954.
13. Bhutada, S.; Goel, M.D. Crashworthiness parameters and their improvement using tubes as an energy absorbing structure: An overview. *Int. J. Crashworthiness* **2022**, *27*, 1569–1600. [CrossRef]
14. Simhachalam, B.; Srinivas, K.; Rao, C.L. Energy absorption characteristics of aluminium alloy AA7XXX and AA6061 tubes subjected to static and dynamic axial load. *Int. J. Crashworthiness* **2014**, *19*, 139–152. [CrossRef]
15. Gao, Z.; Ruan, D. Axial crushing of novel hierarchical multi-cell square tubes. *Eng. Struct.* **2023**, *286*, 116141. [CrossRef]
16. Gao, Z.; Zhang, H.; Zhao, J.; Ruan, D. The axial crushing performance of bio-inspired hierarchical multi-cell hexagonal tubes. *Int. J. Mech. Sci.* **2023**, *239*, 107880. [CrossRef]
17. Malekshahi, A.; Hosseini, M.; Ansari, A.N. Theoretical estimation of axial crushing behavior of multicell hollow sections. *Mech. Based Des. Struct. Mach.* **2022**, *50*, 2591–2615. [CrossRef]
18. Kim, H.S. New extruded multi-cell aluminum profile for maximum crash energy absorption and weight efficiency. *Thin-Walled Struct.* **2002**, *40*, 311–327. [CrossRef]
19. Zhang, X.; Zhang, H.; Yang, C.; Leng, K. Static and dynamic axial crushing of self-locking multi-cell tubes. *Int. J. Impact Eng.* **2019**, *127*, 17–30. [CrossRef]
20. Zhang, Y.; Wang, J.; Wang, C.; Zeng, Y.; Chen, T. Crashworthiness of bionic fractal hierarchical structures. *Mater. Des.* **2018**, *158*, 147–159. [CrossRef]
21. Hu, D.; Wang, Y.; Song, B.; Dang, L.; Zhang, Z. Energy-absorption characteristics of a bionic honeycomb tubular nested structure inspired by bamboo under axial crushing. *Compos. Part B Eng.* **2019**, *162*, 21–32. [CrossRef]
22. Wang, J.; Zhang, Y.; He, N.; Wang, C.H. Crashworthiness behavior of Koch fractal structures. *Mater. Des.* **2018**, *144*, 229–244. [CrossRef]
23. Wang, Z.; Zhang, J.; Li, Z.; Shi, C. On the crashworthiness of bio-inspired hexagonal prismatic tubes under axial compression. *Int. J. Mech. Sci.* **2020**, *186*, 105893. [CrossRef]
24. Chen, B.C.; Zou, M.; Liu, G.M.; Song, J.F.; Wang, H.X. Experimental study on energy absorption of bionic tubes inspired by bamboo structures under axial crushing. *Int. J. Impact Eng.* **2018**, *115*, 48–57. [CrossRef]
25. Hong, W.; Fan, H.; Xia, Z.; Jin, F.; Zhou, Q.; Fang, D.N. Axial crushing behaviors of multi-cell tubes with triangular lattices. *Int. J. Impact Eng.* **2014**, *63*, 106–117. [CrossRef]
26. Zhang, X.; Zhang, H. Energy absorption of multi-cell stub columns under axial compression. *Thin-Walled Struct.* **2013**, *68*, 156–163. [CrossRef]
27. Dong, H.P.; Gao, G.J.; Xie, S.C.; Li, J. Collision performance of bitubular tubes with diaphragms. *J. Cent. South Univ.* **2015**, *22*, 3657–3665. [CrossRef]
28. Ma, W.; Li, Z.; Xie, S. Crashworthiness analysis of thin-walled bio-inspired multi-cell corrugated tubes under quasi-static axial loading. *Eng. Struct.* **2020**, *204*, 110069. [CrossRef]
29. Karagiozova, D.; Shu, D.W.; Lu, G.; Xiang, X. On the energy absorption of tube reinforced foam materials under quasi-static and dynamic compression. *Int. J. Mech. Sci.* **2016**, *105*, 102–116. [CrossRef]
30. Dipaolo, B.P.; Tom, J.G. Effects of ambient temperature on a quasi-static axial-crush configuration response of thin-wall, steel box components. *Thin-Walled Struct.* **2009**, *47*, 984–997. [CrossRef]
31. Tian, Q.L.; Wang, X. The effect of thermal environment on axial crushing load of sandwich tubes. *J. Reinf. Plast. Compos.* **2008**, *27*, 83–101. [CrossRef]
32. Ha, N.S.; Pham, T.M.; Hao, H.; Lu, G.X. Energy absorption characteristics of bio-inspired hierarchical multi-cell square tubes under axial crushing. *Int. J. Mech. Sci.* **2021**, *201*, 106464. [CrossRef]
33. Ye, L.; Lu, G.X. Axial crushing of thin walled cylindrical shell with foam core. *Mater. Res. Innov.* **2011**, *15*, 3–6. [CrossRef]
34. Linul, E.; Lell, D.; Movahedi, N.; Codrean, C.; Fiedler, T. Compressive properties of zinc syntactic foams at elevated temperatures. *Compos. B Eng.* **2019**, *167*, 122–134. [CrossRef]

35. Pham, T.M.; Chen, W.; Kingston, J.; Hao, H. Impact response and energy absorption of single phase syntactic foam. *Compos. B Eng.* **2018**, *150*, 226–233. [CrossRef]
36. Linul, E.; Movahedi, N.; Marsavina, L. The temperature and anisotropy effect on compressive behavior of cylindrical closed-cell aluminum-alloy foams. *J. Alloys Compd.* **2018**, *740*, 1172–1179. [CrossRef]
37. Liang, X.; Luo, H.; Mu, Y.; Chen, M.; Ye, J.; Chi, D. Quasi-static and dynamic compression of aluminum foam at different temperatures. *J. Mater. Eng. Perform.* **2019**, *28*, 4952–4963. [CrossRef]
38. Liu, J.; Qu, Q.; Liu, Y.; Li, R.; Liu, B. Compressive properties of Al-Si-SiC composite foams at elevated temperatures. *J. Alloys Compd.* **2016**, *676*, 239–244. [CrossRef]
39. Taherishargh, M.; Linul, E.; Broxtermann, S.; Fiedler, T. The mechanical properties of expanded perlite-aluminium syntactic foam at elevated temperatures. *J. Alloys Compd.* **2018**, *737*, 590–596. [CrossRef]
40. Wang, P.; Xu, S.; Li, Z.; Yang, J.; Zheng, H.; Hu, S. Temperature effects on the mechanical behavior of aluminum foam under dynamic loading. *Mater. Sci. Eng. A* **2014**, *599*, 174–179. [CrossRef]
41. Wang, S.; Li, W.G.; Tao, Y.; Zhang, X.; Zhang, X.; Li, Y.; Fang, D.N. Investigation on the temperature dependent out-of-plane quasi-static compressive behavior of metallic honeycombs. *Thin-Walled Struct.* **2020**, *149*, 106625. [CrossRef]
42. Wang, L.; Fan, X.; Chen, H.; Liu, W. Axial crush behavior and energy absorption capability of foam-filled GFRP tubes under elevated and high temperatures. *Compos. Struct.* **2016**, *149*, 339–350. [CrossRef]
43. Linul, E.; Movahedi, N.; Marsavina, L. The temperature effect on the axial quasi-static compressive behavior of ex-situ aluminum foam-filled tubes. *Compos. Struct.* **2017**, *180*, 709–722. [CrossRef]
44. Yang, X.; An, T.; Wu, Z.; Zou, T.; Zhao, N. The effect of outer tube on quasi-static compression behavior of aluminum foam-filled tubes. *Compos. Struct.* **2020**, *245*, 112357. [CrossRef]